Hyperfine Interactions 123/124 (1999) 847–861

Inelastic nuclear resonant absorption of synchrotron radiation in thin films and multilayers

W. Keune [a] and W. Sturhahn [b]

[a] *Laboratorium für Angewandte Physik, Gerhard-Mercator-Universität Duisburg, D-47048, Duisburg, Germany*

[b] *Advanced Photon Source, Argonne National Laboratory, Argonne, IL 60439, USA*

Inelastic nuclear resonant absorption of synchrotron radiation is an efficient and unique method for the direct measurement of vibrational density of states (VDOS) of thin films and interfaces that contain Mössbauer isotopes. This is demonstrated for the ^{57}Fe nuclear resonance in the case of amorphous and crystalline Tb–Fe alloy thin films and buried Fe/Cr interfaces in epitaxial α-Fe(0 0 1)/Cr(0 0 1) superlattices.

1. Introduction

The physical properties of thin films and nanoscaled multilayers are a topical subject in a variety of research areas. For instance, new effects have been discovered in thin magnetic films/multilayers that provided new insight into the origin and dynamics of magnetic ordering, perpendicular magnetic anisotropy, and spin-dependent electron scattering leading to giant magnetoresistance (GMR) [1]. Further, metastable crystallographic phases with interesting structural, magnetic or electronic properties have been discovered in epitaxial films on single crystal substrates, e.g., in magnetic 3d-metal films [2] or semiconducting α-Sn films [3].

Surprisingly, studies of such fundamental properties as vibrational excitations in *metallic* thin-film and multilayer systems are scarce. Extensive investigations of phonons in semiconducting epitaxial nanoscaled multilayers (superlattices), mostly performed by Raman spectroscopy, revealed novel phenomena, such as folding of phonon dispersion relations into the Brillouin zone due to the superlattice periodicity, phonon confinement, and vibrational interface states arising at the interface between different layered materials [4]. For metallic multilayers, on the other hand, only few literature reports on folded [5] or confined [6] phonons exist, because most elemental metals are not or are only weakly Raman active. Knowledge of vibrational properties of metallic multilayers is highly desirable, because structural phase transitions or electronic properties may be affected by phonons, e.g., the electrical resistivity by interface phonon scattering [7].

Since the recent discovery of inelastic nuclear resonant absorption of 14.413 keV synchrotron radiation by ^{57}Fe-Mössbauer nuclei in bulk bcc Fe (α-Fe) [8–10], this

technique has evolved as a powerful method to explore atomic vibrational properties of condensed matter not available otherwise. Inelastic nuclear resonant absorption provides a direct measurement of the frequency distribution of lattice vibrations, i.e., of the vibrational density of states (VDOS), for the vibrating Mössbauer isotope in matter. In other words, it is the Mössbauer-isotope projected "partial" VDOS that is directly measured by inelastic nuclear resonant absorption. An excellent recent review of the method is given in [11]. Further details and applications in various fields of science are described by several authors in chapter V of this volume.

Microscopic understanding of thermal properties (e.g., specific heat, thermal expansion), heat transport, and other properties of materials requires knowledge of their atomic vibrational dynamics. One of the key quantities in this sense is the phonon density of states in crystalline solids or (more generally) the vibrational density of states (VDOS) in condensed matter. Important physical quantities, like the Lamb–Mössbauer factor and the average kinetic energy per atom [12] (which is related to the vibrational specific heat), or average atomic force constants and excess potential energy per atom, may be deduced from the VDOS. Peaks in the VDOS are correlated with the low-dispersive sections of the dispersion relations, where the phonon energy is nearly independent of the phonon momentum. Moreover, lattice anharmonicity (responsible for thermal expansion) may be deduced from changes in the VDOS with temperature [11]. Therefore, inelastic nuclear resonant absorption can open a new domain, namely lattice dynamics, in thin-film and multilayer research.

2. Comparison with other techniques

The traditional method for measuring vibrational properties of condensed matter is inelastic neutron scattering (INS) [13] and more recently inelastic X-ray scattering (IXS) [14]. Both methods provide measurements of the fundamental relationship between the vibrational excitation frequency and momentum transfer, i.e., dispersion relations, in bulky solids. From the dispersion curves of single crystals, the phonon density of states (DOS) may be calculated, in principle, by integration over momentum space [15] – a tedious procedure, however. Therefore, inelastic nuclear resonant scattering and INS or IXS provide complementary information. Concerning the understanding of vibrational dynamics from an atomistic point of view, phonon dispersion relations are of more fundamental significance than the VDOS, while the VDOS is of more practical importance.

It is worthwhile mentioning that there are several important differences between INS (and also IXS) and inelastic nuclear resonant absorption. The technique used to measure inelastic nuclear resonant absorption of X-rays via products of internal conversion involves an *incoherent* process with a very large nuclear cross-section [11]. This means that the phase relation between different detected waves (e.g., X-ray fluorescence radiation) is uncorrelated, and *single* particle vibrations of the Mössbauer nuclei *only* can be studied. This allows the direct measurement (with a minimum of modelling [9,11]) of the partial VDOS. By contrast, the measured cross-section in INS

generally contains two contributions: *coherent* scattering (which allows the study of collective atomic vibrations, i.e., dispersion relations) and *incoherent* scattering (which is related to single-particle vibrations and VDOS) [16]. Direct measurements of VDOS from incoherent INS or IXS are difficult (if not impossible) due to the small incoherent cross sections usually involved. In the case of coherent INS, a *generalized* VDOS can be determined with partial contributions according to the scattering power of each element in the sample [16]. However, the data analysis is not so straightforward, due to interference scattering and coherent multiphonon scattering [16]. That inelastic nuclear resonant absorption provides an *isotope-selective* (partial) VDOS has been convincingly demonstrated recently for the case of ^{57}Fe in a bulk Al–Cu–Fe quasicrystal: the iron VDOS was found to be strongly peaked similar to an Einstein oscillator, whereas the generalized neutron VDOS exhibits a different behaviour [17].

Inelastic nuclear resonant absorption is sensitive to the direction of lattice vibrations in anisotropic single crystals [11], and the measured VDOS may become anisotropic in this case. This "projected" VDOS measured with the photon wave vector **k** along a certain crystallographic direction is equal to the usual VDOS weighted by the projection of the phonon polarization vectors **e** to the **k** direction, i.e., $\mathbf{e}\cdot\mathbf{k}/k$ [18]. Similar effects are expected in anisotropic epitaxial thin films. In a random polycrystal, this effect is averaged out. In coherent INS similar considerations apply, but **k** is replaced by **Q**, the unit vector in the direction of the momentum transfer [16], and anisotropy occurs because of interference effects.

Compared with INS and IXS, a significant advantage of inelastic nuclear resonant absorption is the small amount of material required. Due to the small scattering cross-sections, INS and IXS can be performed on bulk samples only; for instance, 10–50 g sample material are necessary for INS [16]. This makes INS and IXS unsuitable for the investigation of atomic dynamics in thin films. However, the situation will improve with the next generation of pulsed neutron sources. On the other hand, energy loss spectroscopy with electrons or He atoms [19] or point-contact methods [20] are intrinsically too surface sensitive. Moreover, phonons with larger wave vectors **q** are difficult to measure with electrons because the cross-section depends on $(1/q)^4$ [16]. Inelastic scattering of visible or infrared light (Brillouin or Raman scattering) has been used extensively to study vibrational excitations in (mostly semiconducting) thin films and multilayers [4,21], but the limited momentum transfer does not allow derivation of the VDOS. Further, the penetration depth of light in metals is small, and thus the scattered intensity is very low and difficult to measure. Accordingly, inelastic nuclear resonant absorption is the most promising method at present for deriving VDOS in thin films and nanoscaled multilayers.

3. Experimental technique

The experimental set-up for measurements of inelastic nuclear resonant absorption has been described in detail in [8–11] and in the article by Chumakov and Sturhahn [22]. The same experimental arrangement is employed in thin film inves-

tigations. The experiments described here were performed at the undulator beam line 3-ID of SRI-CAT at the Advanced Photon Source. The bandwidth of the highly collimated beam of X-rays from the undulator is brought down to a value of the order of an eV by a high-heat-load monochromator that uses two symmetric diamond (1 1 1)-Bragg reflections in a nondispersive arrangement. Further monochromatization down to 5.5 meV or 2.5 meV bandwith is achieved by a high-resolution, nested Si-crystal monochromator [23], as described by Toellner [24]. The synchrotron beam illuminated the ^{57}Fe-containing thin films under a grazing angle of $\approx$4 mrad. The energy was tuned in steps of 0.8 meV around the 14.413 keV nuclear resonance of ^{57}Fe. The typical intensity at 5.5 meV (2.5 meV) was 10^{10} photons/s ($3 \cdot 10^9$ photons/s) in a beam size of 0.5×2 mm^2. An avalanche photodiode was mounted above the thin film and detected the time-delayed characteristic 6.4 keV fluorescence X-rays of iron emitted after the nuclear de-excitation. The measurements were performed with the samples at room temperature (300 K). The collection times were 2–10 h per spectrum for the Tb–Fe alloy films, depending on layer thickness and iron content, and up to about 24 h per spectrum for the Fe/Cr superlattices.

Here, we describe results obtained from inelastic nuclear resonant absorption in amorphous (a-) $Tb_{1-x}Fe_x$-alloy thin films of 17.5 nm thickness with $x =$ 0.30, 0.50, 0.67, 0.77 and 0.82, and of 80 nm thickness with $x = 0.82$. For comparison, we also investigated an 80 nm thick epitaxial (crystalline) $TbFe_2$(1 1 0) film (cubic Laves phase). All alloy thin films were prepared in ultrahigh vacuum by thermal co-evaporation of Tb (99.99% purity) and 95.5% enriched ^{57}Fe metal [25]. The 17.5 nm thick amorphous films were grown at 300 K on oxidized Si(0 0 1) wafers initially coated with a 20 nm thick Pt buffer layer. Reflexion of the synchrotron beam at the Pt layer in grazing incidence enhances the 6.4 keV fluorescence signal of inelastic nuclear resonance absorption in the 17.5 nm thick a-$Tb_{1-x}Fe_x$ overlayer due to a waveguide effect (GIAR effect). For details we refer to the article by Röhlsberger [26]. The 80 nm a-$Tb_{0.18}Tb_{0.82}$ film was grown in the same way, but without a Pt-buffer layer. The $TbFe_2$(1 1 0) film was deposited at 500°C on a sapphire (11–20) substrate which carried a 35 nm Nb(1 1 0) buffer layer and a 1.5 nm ^{57}Fe seed layer on the Nb surface [27]. All samples were coated with $\sim$5 nm Si for protection against oxidation. Figure 1 exhibits typical X-ray diffraction (XRD) patterns of the epitaxial $TbFe_2$ film (top) and of the a-$Tb_{0.33}Fe_{67}$(17.5 nm) film (bottom). This result confirms the $TbFe_2$(1 1 0) epitaxial orientation and the amorphous structure of this Tb–Fe film, respectively; in the latter case only Bragg peaks of the Pt buffer layer and no Bragg reflexions of the amorphous Tb–Fe film are observed. The amorphous structure of all a-$Tb_{1-x}Fe_x$ films was further confirmed by XRD and conversion electron Mössbauer spectroscopy (CEMS) [25].

As another example, we have studied epitaxial Fe(0 0 1)/Cr(0 0 1) superlattices by inelastic nuclear resonant absorption. Two types of Fe/Cr samples (labeled Arg 03 and Arg 04, respectively) were grown in ultrahigh vacuum at 160°C by molecular-beam epitaxy (MBE) on MgO(0 0 1) substrates carrying a 5 nm thick Cr buffer layer which was grown previously at 670°C. Sample Arg 03 had a multilayer period of the type

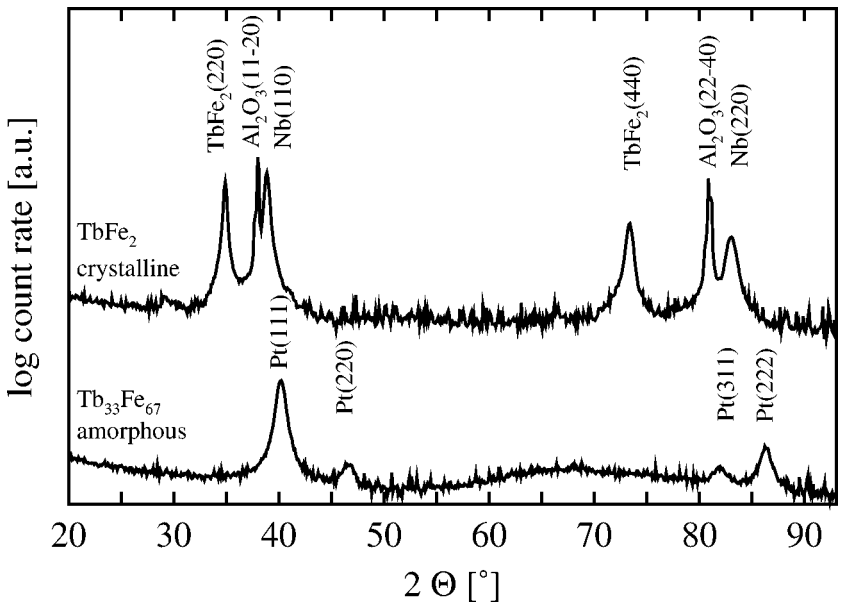

Figure 1. X-ray diffraction patterns of an 80 nm thick epitaxial $TbFe_2(1\,1\,0)$ film grown on a Nb(1 1 0) buffer layer on sapphire (11–20) (top), and of a 17.5 nm thick amorphous $Tb_{0.33}Fe_{0.67}$ alloy film grown on a Pt buffer layer on Si wafer (bottom).

$[^{5}7Fe(0.7\ ML)/^{56}Fe(8\ ML)/Cr(8\ ML)]_{200}$, repeated 200 times (ML = monolayer or atomic layer), while the multilayer period of sample Arg 04 was of the type $[^{56}Fe(4\ ML)/^{57}Fe(0.7\ ML)/^{56}Fe(4\ ML)/Cr(8\ ML)]_{200}$. Isotopically depleted ^{56}Fe was used, which gives no nuclear resonance signal. In addition, 0.7 ML (0.1 nm) thick probe layers (tracer layers) of 95.5% enriched ^{57}Fe were artificially placed either at the ^{56}Fe-on-Cr interfaces (sample Arg 03) or at the center of ^{56}Fe layers (sample Arg 04). This provides a nuclear resonance signal either from this type of Fe/Cr interface (Fe deposited onto Cr) (Arg 03) or from the Fe-film centers (Arg 04). The total ^{57}Fe thickness in each sample is 20.0 nm. The high structural quality of our superlattice samples was demonstrated by large-angle XRD [28], where superlattice satellite reflexions were observed around the Bragg peak.

4. Vibrational density of states

4.1. Tb–Fe alloy thin film

The measured data were normalized according to standard procedures [9,12], and the resulting vibrational excitation probabilities per unit of energy are shown in figure 2. These spectra exhibit a dominant central elastic peak around the nuclear transition energy and side bands at lower and higher energy. X-rays with less energy than the nuclear transition can excite the nuclear resonance by net annihilation of vibrational quanta (low-energy side band). The high-energy side band is produced by

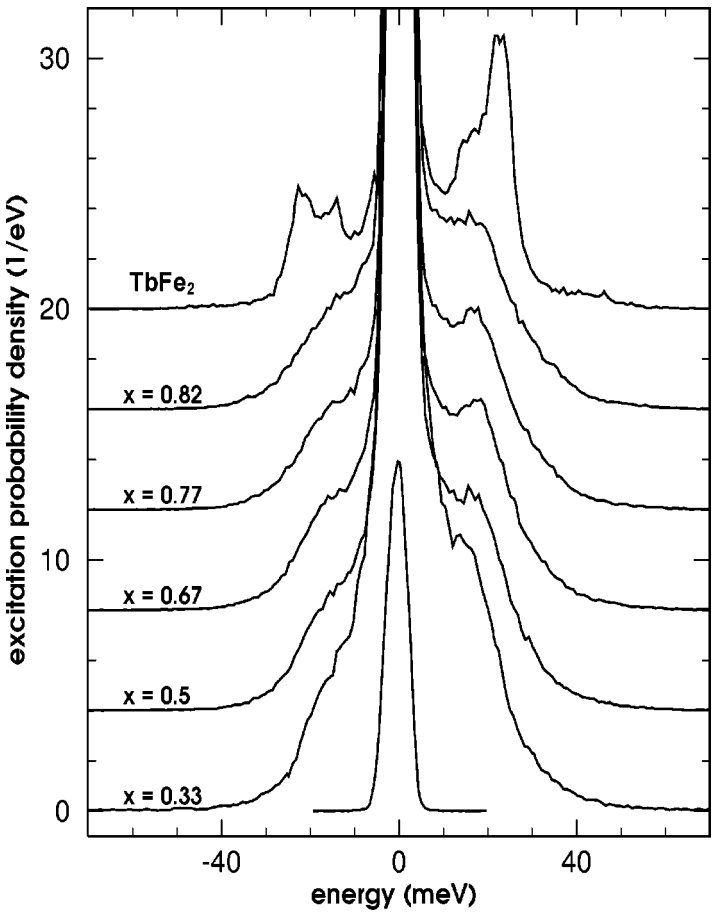

Figure 2. Vibrational excitation probability density versus energy transfer to the lattice. The spectra obtained from the a-$Tb_{1-x}Fe_x$(17.5 nm) films and the crystalline (cubic Laves phase) $TbFe_2$(80 nm) film (top spectrum) soften with decreasing iron content x. The resolution function of the instrument was measured separately and is depicted at the bottom (5.5 meV energy resolution).

creation of vibrational quanta. The observed asymmetry in the spectra reflects the "detailed balance" [29] for the vibrational quanta.

Several moments of the excitation probability density provide important model-independent quantities [12,29] for the iron atoms. The zero-order moment gives the probability for recoilless absorption, i.e., the Lamb–Mössbauer factor (f-factor), the second-order moment gives the average kinetic energy, and the third-order moment provides the average curvature of the potential energy, i.e., the average force constant. In figure 3, we show the moments versus the composition x of the amorphous $Tb_{1-x}Fe_x$ films. Values of bcc-iron metal and of the crystalline Laves phase of $TbFe_2$ are also given. The probability for recoilless absorption (figure 3(a)) and the average force constants (figure 3(c)) increase with the iron concentration x of the amorphous alloys. Linear extrapolation of the measured values to $x = 1$ indicates considerably reduced

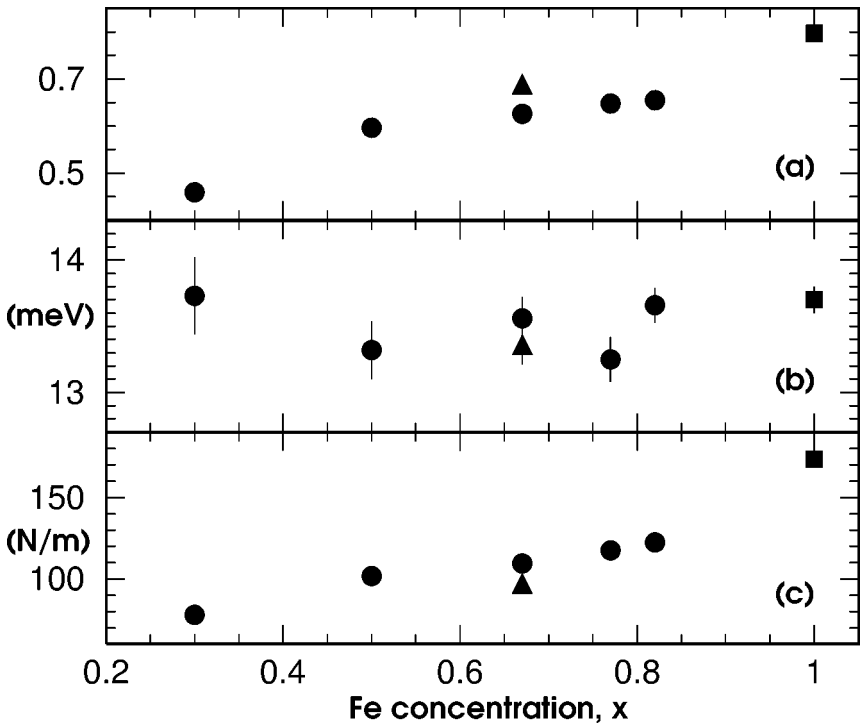

Figure 3. Probability for recoilless absorption (a), average kinetic energy per iron atom (b), and average force contant (c), for a-$Tb_{1-x}Fe_x$ thin films. Values for bcc Fe (squares) and the crystalline $TbFe_2$ film (Laves phase) (triangles) are also given.

values for the f-factor and the average force constant (binding forces) of (hypothetical) pure amorphous iron relative to bcc Fe. On the other hand, the average kinetic energy (figure 3(b)) is essentially the same for all samples, and (by virtue of the virial theorem) we may assume similar behaviour of the average potential energy of the iron atoms. The average kinetic energy of the Fe atom is related to the second-order Doppler shift (SOD) in Mössbauer spectra [12]. This quantity cannot be measured accurately by Mössbauer spectroscopy in the case of a-$Tb_{1-x}Fe_x$ alloys due to the broad distributions of magnetic hyperfine fields and isomer shifts and their correlation. Inelastic nuclear resonant absorption is more precise for the determination of the SOD shift in this case.

The partial VDOS deduced from the excitation probability densities are shown in figure 4. For amorphous $Tb_{1-x}Fe_x$ films, the VDOS represents a structureless broad feature, as anticipated for such an atomically disordered material. Qualitatively similar frequency distributions (more exactly: generalized frequency distributions) have been obtained by coherent inelastic neutron scattering on bulk samples of binary metallic glasses, e.g., a-$Mg_{70}Zn_{30}$ [16]. The maximum energy of the VDOS in figure 4 shifts to lower energies with decreasing Fe content x of the amorphous films, i.e., the Fe vibrations soften with decreasing iron content. The same (partial) VDOS within error bars were measured on 80 and 17.5 nm thick

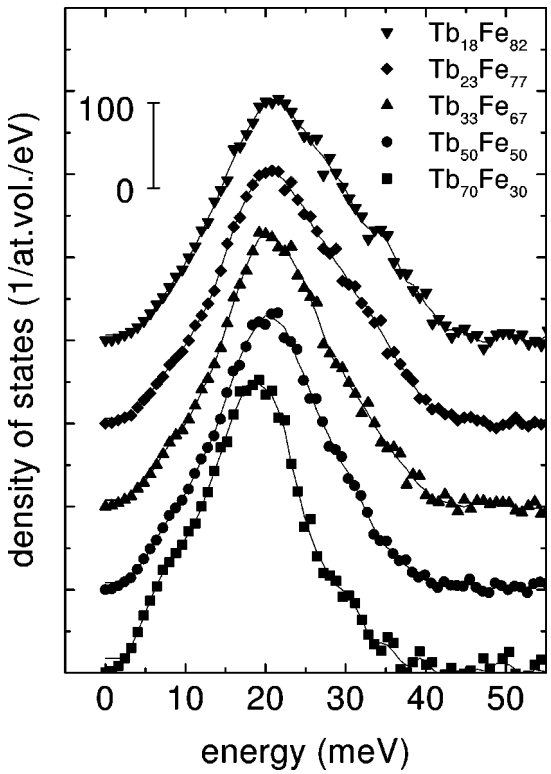

Figure 4. Partial vibrational density of states (VDOS) versus energy of 17.5 nm thick amorphous $Tb_{1-x}Fe_x$ films with decreasing iron content x (from top to bottom) (5.5 meV energy resolution). The drawn lines are a guide for the eye only.

a-$Tb_{18}Fe_{82}$ films (figure 5), i.e., the VDOS does not depend on thickness in this region.

It is interesting to compare the (partial) VDOS of the crystalline (cubic Laves phase) $TbFe_2$ film (80 nm) with the amorphous $Tb_{0.33}Fe_{0.67}$ film (17.5 nm) of the same composition (figure 6) [28]. The partial VDOS of the $TbFe_2$ film exhibits a sharp peak at $\sim$23 meV, as compared to a very broad maximum at $\sim$20 meV of the a-$Tb_{0.33}Fe_{0.67}$ film. Moreover, the partial VDOS of the amorphous film is remarkably higher than that of the crystalline film at lower and higher energies. The distinct shoulder near 15 meV in the VDOS of the Laves phase film is related to longitudinal and transverse acoustic phonon modes, while the main peak near 23 meV is due to optical phonon modes [28]. No equivalent distinct vibrational states exist for iron atoms in the amorphous film. The distinct differences in the partial VDOS of the crystalline $TbFe_2$ film and the a-$Tb_{0.33}Fe_{0.67}$ film illustrate the influence of atomic order versus disorder on the atomic vibrations. Due to its atomic disorder the amorphous structure leads to smearing out of the distinct features in the VDOS of crystals, and even to localized phonons [30]. Similar effects have been found for phonons in nanocrystalline iron [31]. We think that anharmonic effects, like phonon lifetime broadening, are of

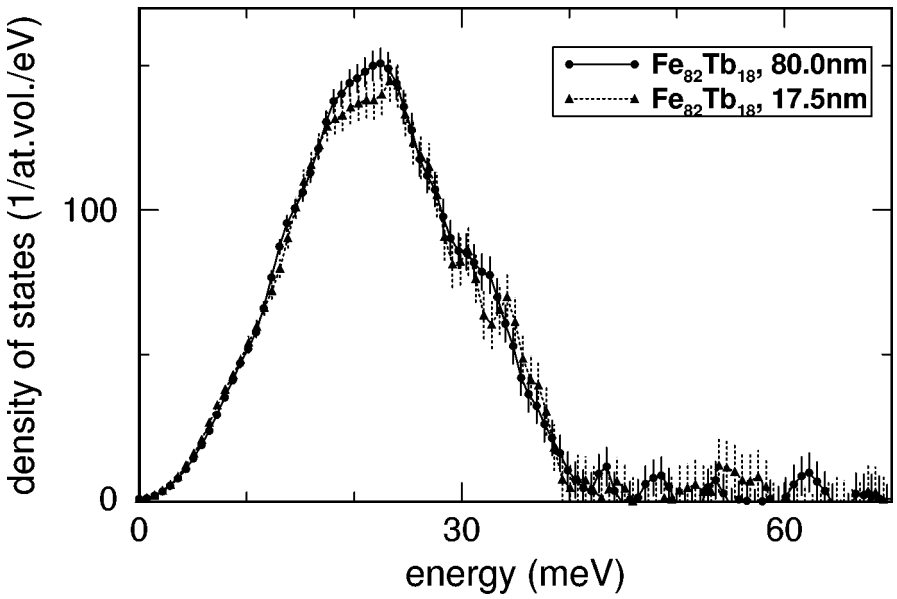

Figure 5. Partial VDOS versus energy for the 17.5 and 80 nm thick a-$Tb_{18}Fe_{82}$ films. No significant difference is observed in this thickness regime (5.5 meV energy resolution).

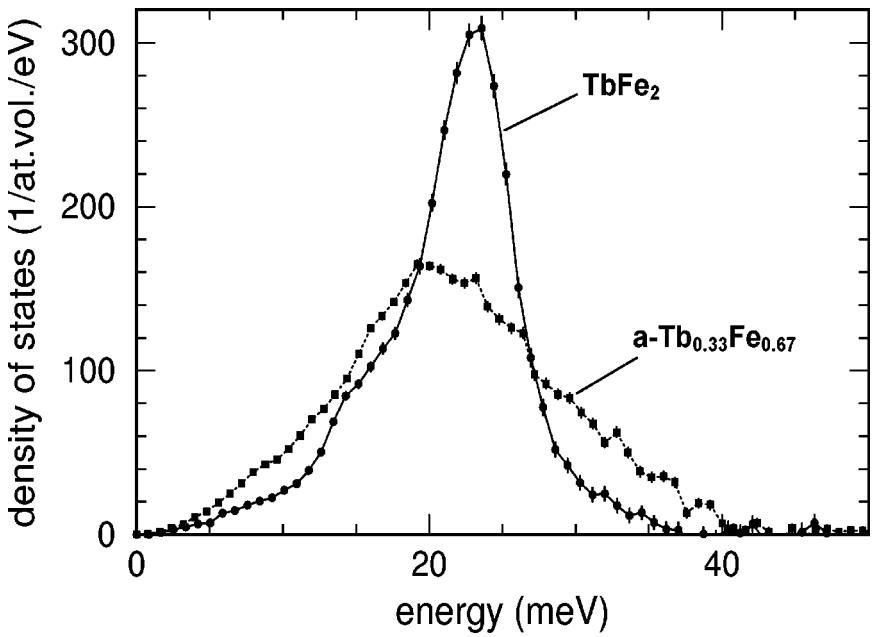

Figure 6. Partial VDOS versus energy of the crystalline (cubic Laves phase) 80 nm thick $TbFe_2$ film (circles) and of the 17.5 nm thick amorphous $Tb_{0.33}Fe_{0.67}$ film (squares) of the same composition (5.5 meV energy resolution).

inferior importance for the VDOS of amorphous systems, since we did not observe important differences in the VDOS of our amorphous films measured at 300 K and at low temperature (10 K). The additional intensity in the VDOS of the amorphous film above 30 meV (figure 6) may be attributed to vibrations of iron atoms that are in regions of shorter distances to their neighbours than those corresponding to the mean density of the amorphous alloy (regions of positive internal pressure), as has been discussed for other binary amorphous alloys [16]; alternatively, this effect may arise from regions where Fe atoms are surrounded by more Fe neighbouring atoms and experience larger binding forces than in the average amorphous alloy. The additional low-frequency modes observed in figure 6 for the amorphous Tb–Fe alloy compared with the crystalline case are of considerable interest, because they might be related to localized vibrational states [32]; alternatively, they might be a precursor of a structural instability in disordered solids [33]. In this respect, measurements with higher energy resolution ($\sim$1–2 meV) are highly desirable in order to extend the reliable measurement region to lower vibrational energies.

Physical vapor deposition methods (such as the one used here) may produce local chemical and structural anisotropies in the amorphous binary alloy. Based on extended X-ray absorption fine structure (EXAFS) measurements [34,35] or conventional X-ray scattering at high X-ray energies as well as anomalous dispersion X-ray scattering [36], structural anisotropy has been shown to exist in amorphous Tb–Fe alloy films deposited at temperatures $\geqslant$300 K by the dc- or rf-magnetron sputtering method. This structural anisotropy was modelled by anisotropic atomic pair correlations, where Fe–Fe pairs are statistically preferred in the film plane and Fe–Tb pairs preferred in the perpendicular direction. The large perpendicular magnetic anisotropy observed in a-Tb–Fe alloy films [34–36] (and also in our MBE-grown a-$Tb_{1-x}Fe_x$ films [25]) was proposed to be the result of this anisotropic local atomic environment. As this structural anisotropy is very small and difficult to observe with the methods mentioned above, we do not believe that it will be detectable in the VDOS by variation of the angle of incidence of the synchrotron beam.

4.2. Epitaxial Fe/Cr(0 0 1) superlattice

Fe/Cr multilayers have been investigated extensively since new phenomena, like indirect magnetic exchange coupling of the Fe layers via the Cr interlayers and giant magnetoresistence (GMR), were observed in this system for the first time [1]. The state of the Fe/Cr interface, whether atomically sharp or interdiffused, influences the exchange coupling strength and the magnitude of the GMR. It is assumed that spin-dependent interface scattering of conduction electrons dominates in the Fe/Cr system, resulting in GMR. As the GMR effect is strongly temperature-dependent, knowledge of the atomic vibrational dynamics at the Fe/Cr interface becomes important for the complete physical understanding of this effect. The antiferromagnetic interlayer coupling of Fe layers via Cr spacer layers has been observed by pure ^{57}Fe-nuclear Bragg diffraction from an Fe/Cr multilayer [37].

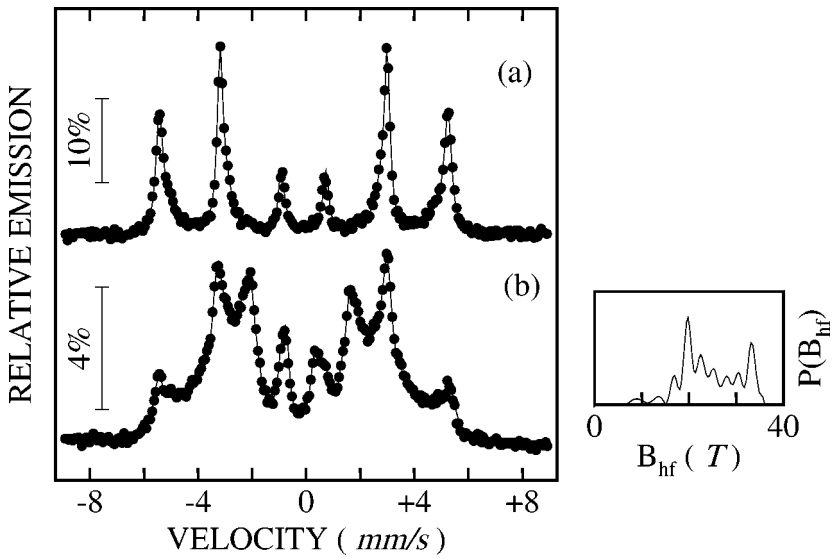

Figure 7. Room-temperature ^{57}Fe conversion-electron Mössbauer spectra (CEMS) from 0.7 ML ^{57}Fe-probe layers in the center of ^{56}Fe layers (sample Arg 04, (a)) or at the ^{56}Fe-on-Cr interfaces (sample Arg 03, (b)) in ^{56}Fe/Cr(0 0 1) superlattices. Right-hand side: magnetic hyperfine-field distribution, $P(B_{\rm hf})$, in sample Arg 03 extracted from a least-squares fit to the spectrum.

A very important question in the context of the VDOS of a buried interface addresses the structural and chemical state of the interface. Probe-layer ^{57}Fe conversion-electron Mössbauer spectroscopy (CEMS) may provide (model-dependent) information on the lateral roughness on an atomic scale of interfaces in Fe/Cr(0 0 1) superlattices [38,39]. The CEM spectrum (figure 7(a)) of our sample Arg 04 (having the 0.7 ML thick ^{57}Fe-probe layer in the center of the ^{56}Fe layers) essentially shows the sharp Zeeman sextet typical of bulk bcc Fe, with narrow lines and a hyperfine field $B_{\rm hf}$ of 33 T at 300 K. Therefore, the ^{57}Fe-probe atoms in the center of the bcc Fe layers (which are ideally 4 ML away from each interface) are essentially unperturbed by the Cr layers. On the other hand, the CEM spectrum of our sample Arg 03 with the 0.7 ML ^{57}Fe-probe layer at the Fe-on-Cr interfaces is a rather complicated superposition of several spectral components, as shown in figure 7(b). This spectrum has been least-squares fitted with a distribution of hyperfine fields, $P(B_{\rm hf})$, shown on the right-hand side of figure 7(b). $P(B_{\rm hf})$ exhibits a number of characteristic peaks due to the various local ^{57}Fe sites. According to the model of [38,39], the peaks observed in the $P(B_{\rm hf})$ distribution are characteristic for ^{57}Fe-probe atoms located on different sites at the interface or inside the "bulk" of the iron layers. The intensities of the components are correlated with the abundances of the various ^{57}Fe sites. In the spectrum of figure 7(b) and its distribution $P(B_{\rm hf})$, there is still a component at $B_{\rm hf} = 33$ T corresponding to bulk-like bcc-Fe sites. Since the ^{57}Fe-probe layer was only 0.7 ML thick, the intensity of the bulk-like component is expected to vanish for the case of atomically perfectly flat and one-monolayer-thick ^{57}Fe patches at the in-

terfaces. However, the $P(B_{\mathrm{hf}})$ peak observed at 33 T in figure 7(b) demonstrates that the interfaces in our sample are not perfectly flat but exhibit some interface roughness on an atomic scale. The most pronounced distribution peak in figure 7(b) is located at a field of ∼19–20 T. According to [38,40], this peak may be attributed to ^{57}Fe sites located within the first atomic layer in ideally flat Fe(0 0 1) terraces directly at the Fe/Cr(0 0 1) interfaces. (Such a site has 4 nearest-neighbour (nn) and 1 next-nearest neighbour (nnn) Cr atoms.) If we believe this assignment, then our sample would contain a reasonable fraction of ideally flat terraces at the Fe/Cr(0 0 1) interfaces, as judged from the large intensity of the $P(B_{\mathrm{hf}})$ peak at ∼19–20 T. However, unfortunately the situation is not so clear, because according to the refined model of [39] a peak near ∼19–20 T alternatively may be assigned to a local ^{57}Fe environment with 4 nn and 2 or 3 nnn Cr atoms. Such a local configuration may arise, for instance, by Cr-impurity atoms within the first ^{57}Fe-atomic layer in ideally flat Fe(0 0 1) terraces directly at the Fe/Cr(0 0 1) interfaces. Therefore, we cannot completely exclude some atomic scale alloying within the first flat ^{57}Fe monolayer directly at the ^{57}Fe-on-Cr interfaces during growth of ^{57}Fe on Cr(0 0 1) at 160°C in our sample. This effect was observed at the unburied Cr/Fe(0 0 1) interface by scanning tunneling microscopy (STM) for the inverse case, i.e., growth of Cr on Fe(0 0 1), at a much higher growth temperature of 300°C, in [41]. Summarizing, we do not assume that the interfaces in our Fe/Cr superlattices are chemically abrupt on an atomic scale, but that they may rather contain atomic Cr impurities (single Cr atoms and/or Cr pairs) dispersed in the first (and perhaps also second) atomic interface layer of the ^{57}Fe overlayer on Cr(0 0 1).

The measured partial VDOS of Fe/Cr samples Arg 03 (interface site) and Arg 04 (center site) exhibit distinct differences, as shown in figure 8. The VDOS of the center site is found to be similar to that of bulk bcc Fe [9]: bulk Fe shows VDOS peaks near 23, 28 and 36 meV, while we observe peaks near 23, ∼26–27 and 36 meV for the film-center site. It is rather striking that the VDOS measured in the center of an embedded 8.7 ML thick bcc-Fe film is so similar to the VDOS of bulk bcc Fe! We should remember, however, that a superlattice is a highly anisotropic system by its very nature and that the X-ray beam impinges at grazing incidence to the film plane, i.e., the direction of the photon wave vector is nearly in the film plane, where no lateral confinement exists for phonons. Because there is an "infinite" lateral extension of the Fe film, its projected VDOS (projected along the parallel photon-wave vector) can be expected to be bulk-like. In order to test this concept, an inelastic nuclear resonant absorption experiment with the photon wave vector perpendicular to the superlattice planes appears to be important. This has not yet been done.

Comparison of the partial VDOS (figure 8) of samples Arg 03 (interface site) and Arg 04 (center site) demonstrates that the VDOS peak of the interface site near 36 meV is remarkably reduced in intensity relative to the center site without changing its energetic position. Moreover, the lower energy feature of the center site around 23–28 meV sharpens and gains in intensity and is shifted to lower energies for the interface site. The partial VDOS of low-energy phonons ($\lesssim$17 meV) are indistinguishable for center and interface Fe sites.

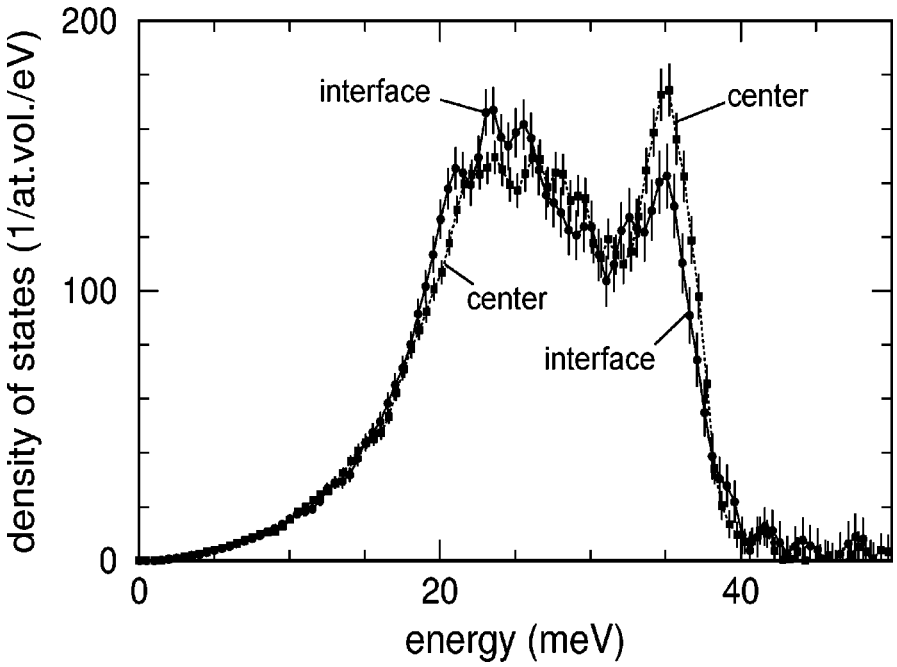

Figure 8. Fe-projected phonon density of states of ^{56}Fe/Cr(0 0 1)-superlattice sample Arg 03 (^{57}Fe interface signal) and sample Arg 04 (^{57}Fe signal from center of ^{56}Fe layers) (2.5 meV energy resolution).

We may speculate about the reason for the reduction of the 36 meV peak intensity at the Fe/Cr interface. One should notice that its position nearly coincides with the deep minimum at ∼34 meV in the VDOS of bulk Cr [42]. Because of this lack of phonon density of states in the Cr layers, part of the Fe phonons near 34 meV remain confined in the Fe films and are suppressed at the Fe/Cr interfaces. Inspection of phonon dispersion curves of bulk Fe and Cr [42] shows that this confinement affects longitudinal [0 0 ζ] phonons of Fe near the H point of the Brillouin zone. We exclude ^{57}Fe-impurity atoms diffused into the Cr layers near the Fe/Cr interfaces as a reason for the observed effect, since the Mössbauer spectrum of ^{57}Fe-interface probe atoms (figure 7(b)) does not show the central single-line component typical for ^{57}Fe impurities in Cr.

The reason for the enhancement of the lower energy VDOS feature at the interface is not clear at present. In bulk Fe, the peak at 23 meV originates from a pronounced minimum in the dispersion curve near the center of the Brillouin zone for longitudinal phonons along the path $\Gamma \rightarrow$ P $\rightarrow$ H [42]. In the same q-space region bulk Cr exhibits a flat longitudinal phonon branch (higher in energy than that of Fe) with a corresponding high Cr VDOS near 32 meV. It seems as if, in this q region and only for interface Fe atoms, the high Cr VDOS is mixed into the Fe VDOS by hybridization, thus increasing the Fe VDOS at the interface. A similar but opposite effect might be responsible for the observed decrease of the Fe VDOS near 28 meV at the interface, involving transverse phonons at the N point. We are aware that these considerations

are rather speculative. Therefore, calculations of the phonon density of states at Fe/Cr interfaces are highly desirable.

5. Conclusions

We have demonstrated in this article that inelastic nuclear resonant absorption of synchrotron radiation via the 14.413 keV ^{57}Fe-nuclear transition is a unique method for the direct measurement of Fe-projected vibrational density of states (VDOS) in metallic crystalline and amorphous thin films, multilayers and isotopically enriched buried interfaces. At the Advanced Photon Source (Argonne National Laboratory), practical measurement times are achieved with an effective total ^{57}Fe thickness in the samples of the order of only $\sim$10 nm. The method may be extended to other isotopes (e.g., ^{119}Sn, ^{151}Eu). This opens vibrational dynamics as a new domain in thin-film multilayer and interface research.

Acknowledgements

The authors are grateful to the staff of the beamline 3-ID of SRI-CAT at the Advanced Photon Source (Argonne) and to T. Ruckert (Duisburg) for participation in the experiments described here and for valuable discussions. We thank U. von Hörsten (Duisburg) for preparing the samples with great expertise. The work at Argonne is supported by the U.S. Department of Energy BES-Materials Science under Contract No. W-31-109-ENG-38. The work at Duisburg was supported by the Deutsche Forschungsgemeinschaft (SFB 166). W.K. is grateful to the Volkswagen Stiftung for supporting his sabbatical stay at Argonne.

References

[1] B. Heinrich and J.A.C. Bland (eds.), *Ultrathin Magnetic Structures*, Vols. I, II (Springer, Berlin, 1994).
[2] G.A. Prinz, J. Magn. Magn. Mater. 100 (1991) 469.
[3] W.T. Yuen, W.K. Liu, S.N. Holmes and R.A. Stradling, Semicond. Sci. Technol. 4 (1989) 819.
[4] B. Jusserand and M. Cardona, in: *Light Scattering in Solids V*, eds. M. Cardona and G. Güntherodt, Topics of Applied Physics (Springer, Berlin, 1989) p. 49.
[5] H. Xia, G.X. Cheng, A. Hu and X.K. Zhang, Solid State Commun. 77 (1991) 631.
[6] M. Grimsditch, J.E. Mattson, C.H. Sowers, S.D. Bader and M.J. Peters, Phys. Rev. Lett. 77 (1996) 2025.
[7] S. Kim, H. Suhl and I.K. Schuller, Phys. Rev. Lett. 78 (1997) 322.
[8] M. Seto, Y. Yoda, S. Kikuta, X.W. Zhang and A. Ando, Phys. Rev. Lett. 74 (1995) 3828.
[9] W. Sturhahn, T.S. Toellner, E.E. Alp, X.W. Zhang, M. Ando, Y. Yoda, S. Kikuta, M. Seto, C.W. Kimball and B. Dabrowski, Phys. Rev. Lett. 74 (1995) 3832.
[10] A.I. Chumakov, R. Rüffer, H. Grünsteudel, H.F. Grünsteudel, G. Grübel, J. Metge, O. Leupold and H.A. Goodwin, Europhys. Lett. 30 (1995) 427.
[11] A. Chumakov and R. Rüffer, Hyp. Interact. 113 (1998) 59.

[12] W. Sturhahn and A. Chumakov, this issue, section V-1.2.
[13] P. Bruesch, *Phonons: Theory and Experiment II* (Springer, Berlin, 1985).
[14] E. Burkel, *Inelastic Scattering of X-Rays with Very High Energy Resolution* (Springer, Berlin, 1991).
[15] N.W. Ashcroft and N.D. Mermin, *Solid State Physics* (Saunders, Philadelphia, PA, 1976) p. 464.
[16] J.-B. Suck and H. Rudin, in: *Glassy Metals II*, eds. H. Beck and H.-J. Güntherodt, Topics in Applied Physics, Vol. 53 (Springer, Berlin, 1983) p. 217.
[17] R.A. Brand, G. Coddens, A.I. Chumakov and Y. Calvayrac, Phys. Rev. B 59 (1999) R14145.
[18] V.G. Kohn, A.I. Chumakov and R. Rüffer, Phys. Rev. B 58 (1998) 8437.
[19] W. Kress and F.W. de Wette (eds.), *Surface Phonons* (Springer, Berlin 1991).
[20] A.V. Khotkevich and I.K. Yanson, *Atlas of Point Contact Spectra of Electron-Phonon Interactions in Metals* (Kluwer, Dordrecht, 1995).
[21] F. Nizzoli and J.R. Sandercock, in: *Dynamical Properties of Solids*, Vol. 6 (North-Holland, Amsterdam, 1990).
[22] A. Chumakov and W. Sturhahn, this issue, section V-1.1.
[23] T.M. Mooney, T.S. Toellner, W. Sturhahn, E.E. Alp and S.D. Shastri, Nucl. Instrum. Methods A 347 (1994) 348.
[24] T.S. Toellner, this issue, section VI-1.
[25] T. Ruckert, J. Tappert, R.A. Brand and W. Keune, J. Magn. Magn. Mater. 165 (1997) 411.
[26] R. Röhlsberger, this issue, section IV-1.3.
[27] V. Oderno, C. Dufour, K. Dumesnil, Ph. Mangin and G. Marchal, J. Chrystal Growth 165 (1996) 175.
[28] W. Sturhahn, R. Roehlsberger, E.E. Alp, T. Ruckert, H. Schrör and W. Keune, J. Magn. Magn. Mater. 198–199 (1999) 590.
[29] W. Sturhahn and V.G. Kohn, this issue, section III-2.2.
[30] J.W. Kantelhardt, A. Bunde and L. Schweitzer, Phys. Rev. Lett. 81 (1998) 4907.
[31] B. Fultz, C.C. Ahn, E.E. Alp, W. Sturhahn and T.S. Toellner, Phys. Rev. Lett. 79 (1997) 937.
[32] G.P. Srivastava, *The Physics of Phonons* (Adam Hilger, Bristol, 1990) p. 318.
[33] W. Schirmacher, G. Diezemann and C. Ganter, Phys. Rev. Lett. 81 (1998) 136.
[34] V.G. Harris, F. Hellman, W.T. Elam and N.C. Koon, J. Appl. Phys. 73 (1993) 5785;
V.G. Harris, W.T. Elam, N.C. Koon and F. Hellman, Phys. Rev. B 49 (1994) 3637.
[35] Y. Fujiwara, X.Y. Yu, S. Tsunashima, S. Iwata, M. Sakurai and K. Suzuki, J. Appl. Phys. 79 (1996) 6270.
[36] T.C. Hufnagel, S. Brennan, P. Zschak and B.M. Clemens, Phys. Rev. B 53 (1996) 12024.
[37] T.S. Toellner, W. Sturhahn, R. Röhlsberger, E.E. Alp, C.H. Sowers and E.E. Fullerton, Phys. Rev. Lett. 74 (1995) 3475.
[38] J. Landes, Ch. Sauer, R.A. Brand, W. Zinn, S. Mantl and Zs. Kajcsos, J. Magn. Magn. Mater. 86 (1990) 71.
[39] F. Klinkhammer, Ch. Sauer, E. Yu. Tsymbal, S. Handschuh, Q. Leng and W. Zinn, J. Magn. Magn. Mater. 161 (1996) 49.
[40] R. Schad, P. Belien, G. Verbanck, K. Temst, V.V. Moshchalkov, Y. Bruynseraede, D. Bahr, J. Falta, J. Dekoster and G. Langouche, Europhys. Lett. 44 (1998) 379.
[41] A. Davies, J.A. Stroscio, D.T. Pierce and R.J. Celotta, Phys. Rev. Lett. 76 (1996) 4175.
[42] W. Kress, *Phonon Disperson Curves, One-Phonon Densities of States and Impurity Vibrations of Metallic Systems*, Physics Data, Vol. 26-1 (Fachinformationszentrum Karlsruhe, Karlsruhe, 1987).